Interaction of Orographic Disturbance with Front①

Wang Xingbao (王兴宝) and Wu Rongsheng (伍荣生)
Department of Atmospheric Sciences, Nanjing University, Nanjing 210093

(Received July 16, 1998; revised November 24, 1998)

ABSTRACT

The interaction of orographic disturbance with front is investigated with a nonhydrostatic fully compressible mesoscale model (ARPS). It is shown that the front is dominated mainly by the orographic disturbance if the front is weak. Firstly, because the stratified airstream is forced to flow along the topographic surface, the topographic surface almost coincides with the lowest isentrope for the barotropic flow. The potential temperature gradients are opposite on upwind slope and downwind slope. As the cold front moves across the mountain, its intensity decreases on the upwind side and increases on the downwind side due to the thermal superposition. Conversely, the warm front is strengthened on the upwind slope and weakened on the downwind slope. This is the thermal superposition effect. Secondly, the mountain-forced circulation and orographic waves, which depend on the shape and size of topography and characteristics of airflow, contribute to frontogenesis and/or frontolysis. This is referred as dynamical action. For the mesoscale mountain ridge of gentle slope, the dynamical action weakens the cold front on the upwind slope, and strengthens the cold front on the lee side. While for the mesoscale mountain of steep slope, the dynamical effect weakens the cold front on the upwind side and strengthens the cold front on the mountain top, the frontal intensity is decreased when front moves downslope rapidly. As front moves into the convergent zone near the mountain base, its intensity is enhanced severely. If the front is intensive, there is strong interaction between the orographic disturbance and the front. The cold front dramatically increases downslope wind and lee side gravity wave activity. And these in turn act upon the frontal intensity and frontal structure. For the baroclinic basic flow, the southerly warm advection on the upwind side makes the cold front less frontolysis; the northerly on the lee side violently intensifies the clod front.

Key words: Orographic disturbance, Front, Interaction

1. Introduction

The importance of orographic effects on front was recognized in the early 20th century. But for the complexity of this problem, the investigation of orographic effects on front from dynamical viewpoint is not taken until the 1980s. Bannon (1983) derived analytical solutions for the quasi-geostrophic front forced by a horizontal wind deformation field that moves over a two-dimensional mountain ridge. The solutions show that as a cold front approaches the ridge, it weakens, relative to the flat-bottom solution, and the front strengthens as it moves down to the lee slope. This effect is the result of superposition of the frontal and mountain-forced temperature fields. The quasi-geostrophic frontal solutions in this case have no dynamic interaction with the mountain solutions because the equations are linear. Zehnder and Bannon (1988) studied the effects of topography on fronts with the semi-geostrophic numerical model. The dynamic interaction between the mountain circulation and the

①The authors acknowledge the support from " Program for the Formation Mechanism and Prediction Theory of Severe Weather Disaster in China" and NSF 49735180.

front can be isolated by subtracting the steady-state mountain solution from the complete solution. They found that the temperature gradient weakens as the front moves up to the mountain slope and strengthens as it moves down to the lee slope. Lu and Nong (1995) got the similar results by means of the semi-geostrophic numerical model.

The resulting solutions of the semi-geostrophic model show the important effects of the ageostrophic advections, which are neglected in the quasi-geostrophic model, on a front as it moves over the ridge. However, in the real atmosphere, flow over the mesoscale mountain with the steep slope would result in significant gravity wave generation. In this case, the non-geostrophic acceleration forced by the topography is not negligible comparing with Coriolis force and the semi-geostrophic approximation breaks down. The interaction of front and mountain must be examined with a primitive equation model. Williams et al. (1992) used the hydrostatic two-dimensional Boussinesq primitive model with the sinusoidal deformation field and the periodic lateral boundary condition in a cyclic domain to study the effects of a mountain on passing fronts. Various mountains were considered. However, the fronts in their model were not realistic to the atmospheric front because they used a sinusoidal temperature field to represent the front. And the hydrostatic approximation may cause severe misrepresentation near the steep mountain slope. Xiao et al. (1997) investigated the deformation frontogenesis with an anelastic nonhydrostatic model incorporating topography. They found that frontolysis exists on the upwind side, slight frontogenesis appears on the downslope side, and severe frontogenesis after the cold front passing the mountain foot downstream.

All these studies have provided the basic dynamics of a front passing over a mountain. However, there are still some limitations and shortcomings. For example, in China the observations indicate that some cold fronts moving from northwest plateau to southeast undergo frontolysis first on the downslope and then frontogenesis again after they move to the plain in the northern China (Zhu et al., 1992). Secondly, in the real atmosphere, after the fronts experience frontogenesis under the action of certain synoptic condition, they maintain a quasi-steady mature state for a longer period, so to study the effects of topography on mature fronts is a matter of more significance. Moreover, it is observed that some severe weather, such as lee cyclone genesis and downslope storm, may occur as the front passing over the mountain. What roles are played by the front for these phenomena? All of the topics require further investigation.

A two-dimensional nonhydrostatic mesoscale model (ARPS) is used to study the above-mentioned problems. The model and the initial condition are briefly described in Section 2. The barotropic and baroclinic flow over the two-dimensional ridge is presented in Section 3. The simulations of front over topography and the frontogenetical function diagnosis are carried out in Section 4. The results and discussions are presented in Section 5.

2. ARPS model description and initial field design

ARPS (Advanced Regional Prediction System) is a nonhydrostatic fully compressible storm- and meso-scale prediction model developed at the Center for Analysis and Prediction of Storms (CAPS), University of Oklahoma. It uses a generalized terrain-following coordinate system. A variety of physical processes are taken into account in the model system including momentum, heat (potential temperature), mass (pressure), water substances, turbulent kinetic energy (TKE), and the equation of state. They are solved on a standard Arakawa C grid with a spilt-explicit solution technique in which the acoustic modes are explicitly inte-

grated with a forward–backward scheme on small time steps. The equations are discretized with fourth–order centered spatial differences and integrated on large time steps with the leapfrog scheme and a Robert–Asselin time filter. A complete description of the model including the governing equations, initialization, boundary condition options, discretizations, and numerical solution techniques can be found in the ARPS Version 4.0 User's Guide (Xue et al., 1995). In this paper the two–dimensional (x–z section) option of the model is selected and basic flow in x direction is added. Take open lateral boundary condition and Rayleigh damping in the upper layer of the model in order to decrease wave reflection. The horizontal grid length of the numerical model is 30 km, and the horizontal model domain is 3780 km. The vertical domain is 16 km. Vertical coordinate is stretched and divided into 35 nonuniform layers. The grid length is enlarged gradually from 50 m at the bottom layer to 950 m at the top layer. The 30 km horizontal grid length is a compromise between resolution and model domain within the limits of computer. The amount of numerical calculation for the nonhydrostatic model may be larger than the hydrostatic model, but the nonhydrostatic model is more flexible and adjustable to unbalanced initial condition and steep topography even at the 30 km grid length. Moreover, along with the increasing of the horizontal grid length, the value of vertical acceleration, dw/dt, will decrease, then the nonhydrostatic results will tend toward the hydrostatic results. In this study the friction and moist process are excluded. The mountain profile is a "witch of Agnesi" which is often used by the theoretical study (Queney, 1948).

$$h = h_m / \left[1 + \left(\frac{x - x_c}{a}\right)^2\right], \tag{1}$$

where h_m is the maximum mountain height, a the mountain half–width, x_c the x coordinate of the maximum mountain height. Assuming that the basic flow, density and pressure field satisfied static equilibrium and geostrophic relation, $\frac{\partial \bar{p}}{\partial z} = -\bar{\rho} g$, $\frac{\partial \bar{p}}{\partial y} = -f\bar{\rho} U_g$, then from the equation of state $\bar{p} = \bar{\rho} R \bar{T}$, $\bar{\theta} = \bar{T}(p_0/\bar{p})^{R/C_p}$, we obtain the following thermal wind relation

$$\frac{g}{\bar{\theta}} \frac{\partial \bar{\theta}}{\partial y} = -f \frac{\partial U_g}{\partial z} + f \frac{N^2}{g} U_g, \tag{2}$$

where $N^2 = \frac{g}{\bar{\theta}} \frac{\partial \bar{\theta}}{\partial z}$, taking $N^2 = 10^{-4}\ \mathrm{s}^{-2}$ in the troposphere ($z < 11$ km), and $N^2 = 4 \times 10^{-4}\ \mathrm{s}^{-2}$ in the stratosphere ($z > 11$ km). Assume $\frac{g}{\bar{\theta}} \frac{\partial \bar{\theta}}{\partial y} =$ constant. Following Orlanski and Ross (1977) the initial along front geostrophic wind is assumed as:

$$v_f = -\frac{x_0}{L_f} V_s \{1 - \tanh[\beta(x_0 - x_f) + \alpha z]\} + V_j \exp\{-[(z - z_j)/L_z]^2 - [(x_0 - x_j)/L_x]^2\}, \tag{3}$$

where x_0 is the x coordinate of model center. $L_f, V_s, \beta, x_f, \alpha, V_j, z_j, L_z, x_j, L_x$ are parameters determining the front. The different values of these parameters will display different frontal structure. Unless declare particularly, we take

$L_f = 10^6$ m, $\beta = 2 \times 10^{-5}\ \mathrm{m}^{-1}$, $\alpha = 2 \times 10^{-3}\ \mathrm{m}^{-1}$, $x_j = 10^6$ m, $z_j = 1.5 \times 10^3$ m, $L_z = 2 \times 10^3$ m,

$x_j = x_f + 3 \times 10^5$ m , $L_x = 2 \times 10^3$ m , V_s, V_j are to be determined later.

From the expression of v_f, we can determine v_g at $z = 0$. Let $U_g = U_s$ at $z = 0$. If the potential temperature on the ground and the stratification are given, then the initial potential temperature, pressure and wind fields in the whole model domain can be acquired from the equation of static equilibrium, geostrophic wind relation and equation of state.

3. Barotropic and baroclinic flow over mountains and their comparisons with semi-geostrophic solution

In order to understand the influence of the mountain on fronts, it is necessary to find mountain solution without front using the same model. However, the solution of flow over a mountain depends on the size and shape of mountain, stratification and speed of airflow. Moreover the baroclinic flow possesses different properties from the barotropic flow (Bannon and Zehnder, 1989). Scale analysis indicates that nondimensional parameters, the Froude number $Fr = U / Nh_m$ and the Rossby number $Ro = U / (fa)$, are essential in the study of stratified flow over topography. In the case of small ridge height ($Fr \gg 1$) linear theory provides a useful indication of the response (Smith, 1986). The orographic disturbances are mainly the climbing flow and the mountain waves. When $Fr \ll 1$, the mountain is very high and / or the stratification is strong, the flow is highly nonlinear. In this case the flow is mainly confined to horizontal planes diverting around rather than climbs the mountain (Drazin, 1961). For $Ro \gg 1$, the earth's rotation has little effect, and the theory of the resulting gravity wave pattern can be simplified by ignoring the rotation. If the flow climbs over extensive mountain areas of small Rossby numbers ($Ro \ll 1$), simplification is achieved by utilizing the quasi- or semi-geostrophic character of the flow. In the middle range, $Ro \sim 1$, $Fr \sim 1$, at normal wind velocities, this would correspond to mountains with half- width of the order of a hundred or a few hundred kilometers, here termed mesoscale. The dominant perturbations take the form of inertia-buoyancy wave and / or pseudo-geostrophic waves and both of them are associated with comparatively large amplitude. The nonlinear effect is not negligible and the quasi- or semi- geostrophic approximations cannot be utilized. So comparatively less effort has been made to investigate in detail this parameter space. However, these kinds of topography have very important influences on fronts. There have been great advances since the ALPS Experiment (ALPEX), but the interactions of front with mesoscale mountains still need to be further studied (Smith, 1986; Blumen, 1992).

Table 1. The parameters concerning the flow over mountain

Case	Airflow	Stratification	Orography	Fr	Ro	$\mu = Ro / Fr$
EX1	$U = 10$ m / s	$N = 0.01$ s^{-1}	$h_m = 2$ km, a = 200 km	0.5	0.5	1
EX2	$U = 10$ m / s	$N = 0.01$ s^{-1}	$h_m = 2$ km, a = 500 km	0.5	0.2	0.4
EX3	$U = 10 + 0.003z$ m / s	$N = 0.01$ s^{-1}	$h_m = 2$ km, $a = 200$ km	>0.5	>0.5	~1
EX4	$U = 10 + 0.003z$ m / s	$N = 0.01$ s^{-1}	$h_m = 2$ km, $a = 500$ km	>0.5	>0.2	~0.4

Where $\mu = Ro / Fr = (N / f)(h_m / a) = h_m / D$ is the nondimensional mountain height.

For long mountain ridge satisfying $Ro \sim 1$, $Fr \sim 1$, the three-dimensionality is not very strong, so the two-dimensional numerical model can be utilized. In order to investigate the frontal interactions with mesoscale topography, at first we consider the problem of airflow over this kind of mountains without front. Some numerical experiments have been performed

for different mountain heights, widths and flow speeds (as a result of the different Froude numbers and Rossby numbers). The results show that the larger the Rossby number, the higher the speed of the ageostrophic wind of the orographic disturbances for a given Froude number. This indicates that the ageostrophic motion is enhanced with the increasing of the Rossby number. It is also found that smaller Froude number is in favor of topographic blocking and stronger downslope wind in the lee side for given Rossby number. But the small Froude number prevents the disturbances from propagating to higher level. To save space only a few experiments are given below. The parameters in the experiments are listed in Table 1

After the parameters have been fixed, the profile of topography, the basic flow and the potential temperature can be obtained from (1) and (2). With these fields as initial condition the model is integrated for 72 hours. The mountain-generated disturbances will be classified into three categories: 1) A downstream-propagating disturbance caused by impulsive flow switching on, 2) an upward-propagating inertia-gravitational wave located over mountain which tends to become stationary lee wave after a long time, 3) a weak upstream-propagating layer (thickness~ h_m) of decelerated fluid. At $t \sim 10\ a/U$, the disturbances reach quasi-steady state. Figure 1 shows the potential temperature, horizontal divergence and vertical velocity fields of EX1, EX2, EX3, EX4 at 48 hours which have few differences from the 72-hour results.

The potential temperature in Fig. 1 consists of a cold orographic anomaly. The isentropes in EX1 and EX2 represent the flow over the mountain ridge. Since the potential temperature is constant along a trajectory in steady state, the topographic surface should coincide with the lowest isentrope for the barotropic flow. The isentrope intersects with the topography for the baroclinic shear flow, because the northward (southward) flow on the upslope (downslope) side produces warm (cold) air advection that partially compensates the adiabatic cooling (warming) by forced ascent (descend) (see EX3 and EX4). The fields are clearly asymmetric with respect to the crest of the ridge in all fields. The u component is stronger and is shifted onto the lee slope relative to the semi-geostrophic solution (figure omitted). For the steeper slope mesoscale mountains, the cross-mountain acceleration increases dramatically and the speed maximum is advected down to the lee side slope. When it reaches the base of the topography, a hydraulic jump is generated near the surface. The v filed contains a region of cyclone shear on the lee slope, which appears to be caused by the strong convergence in the u field. However, the fields of steady solution for the semi-geostrophic flow over mountain are of symmetry with respect to the crest of ridge. Its maximum zonal velocity occurs at the mountain top. The flow is weakly convergent at the upwind base of the mountain, divergent on the upslope, and convergent on the downslope (Bannon and Zehnder, 1989). It is clear from these solutions that the semi-geostrophic equations are not accurate for these mountains, especially for the steep mountain, the hydraulic jump and the wave activity are present on the lee side. Later it will be shown that these characteristics of airflow influence the front markedly. In addition, EX3, EX4 compared with EX1, EX2 demonstrates that the baroclinic flow is in favor of upward development of disturbances.

4. Frontal interactions with topography

The impulsive input of topography in the zonal flow generates transient wave. Because it is caused by the unrealistic initial condition, its influence should be reduced as much as possible. Many investigators usually take the steady semi-geostrophic solution of flow over mountain as initial condition. However, for the mesoscale topography the semi-geostrophic

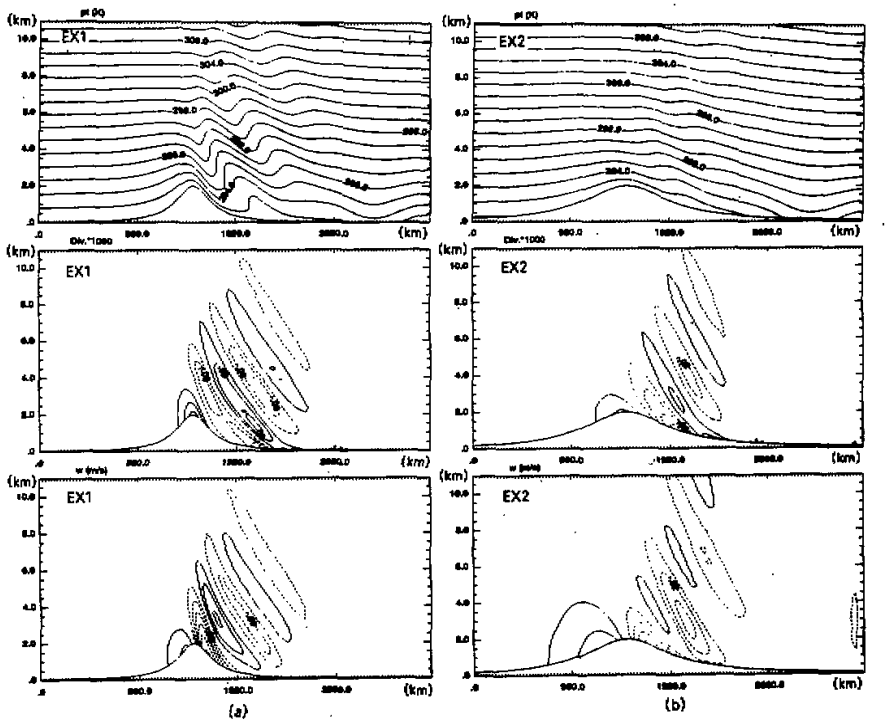

(a) and (b) corresponding to EX1, EX2 respectively

Fig. 1. Quasi-steady state of orographic barotropic / baroclinic flow response for different mountain widths. Displayed are the $x-z$ cross-sectional distribution of potential temperature at left panel, horizontal divergence at middle panel, and vertical velocity at right panel.

solution cannot eliminate the transient wave completely. In this paper we will firstly integrate the model from impulsive initial condition to quasi-steady state for about 48 hours. Then take the sum of the quasi-steady state and the frontal disturbance as initial condition and integrate the model for 72 hours. Some of the experiments are listed in Table 2.

Table 2. The parameters for the interaction between front and topography

Case	Airflow	Front	Orography	*Fr*	*Ro*	$\mu = Ro/Fr$
FEX1	$U = 10$ m/s	$V_s = 10$ m/s, $V_j = 0$ m/s	$h_m = 2$ km, $a = 200$ km	0.5	0.5	1
FEX2	$U = 10$ m/s	$V_s = 10$ m/s, $V_j = 0$ m/s	$h_m = 2$ km, $a = 500$ km	0.5	0.2	0.4
FEX3	$U = 10 + 0.003z$ m/s	$V_s = 10$ m/s, $V_j = 0$ m/s	$h_m = 2$ km, $a = 200$ km	>0.5	>0.5	~1
FEX4	$U = 10$ m/s	$V_s = 10$ m/s, $V_j = 15$ m/s	$h_m = 2$ km, $a = 200$ km	0.5	0.5	1
FEX5	$U = 10 + 0.003z$ m/s	$V_s = 10$ m/s, $V_j = 15$ m/s	$h_m = 2$ km, $a = 200$ km	0.5	0.5	1

In all experiments $N = 0.01$ s^{-1}.

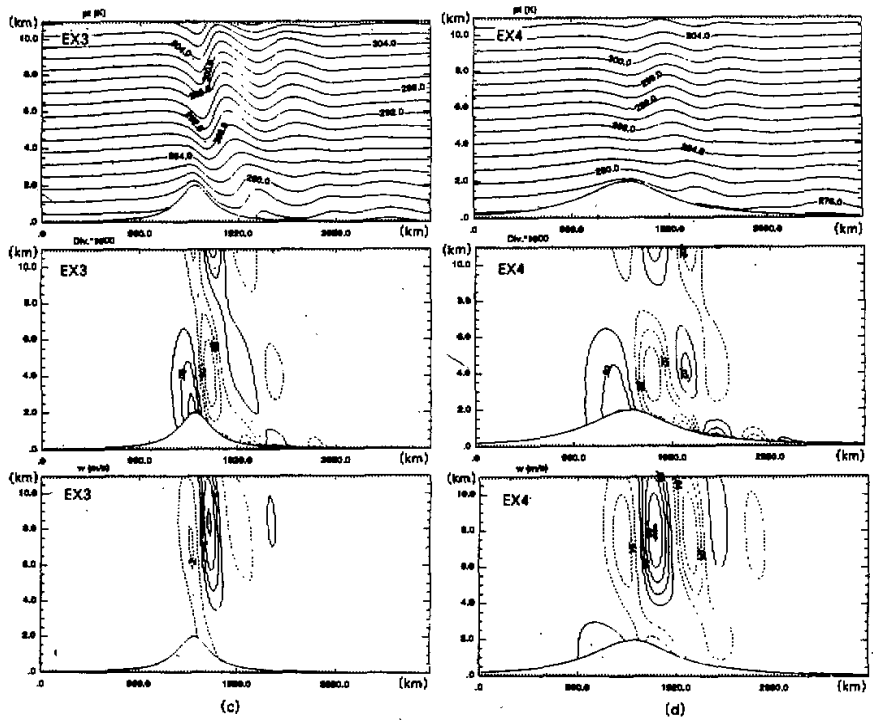

(c) and (d) corresponding to EX3, EX4 respectively

4.1 *Frontal solutions without topography*

As control runs for the later solutions with topography, the frontal solutions without topography for different initial frontal intensities in barotropic and baroclinic flows are tested respectively. For the convenience of discussion we symbolize $U=10$ m/s, $V_s=10$ m/s, $V_j=0$ m/s case as FCL1, $U=10$ m/s, $V_s=10$ m/s, $V_j=15$ m/s case as FCL2, $U=10+0.003z$ m/s, $V_s=10$ m/s, $V_j=0$ m/s case as FCL3 and $U=10+0.003z$ m/s, $V_s=10$ m/s, $V_j=15$ m/s case as FCL4. And in all the four experiments $N=0.01$ s^{-1}. Since the limit of the resolution of the model and the dissipation due to the numerical discretization, the gradient of the potential temperature in frontal zone is decreasing with time in FCL1 and FCL2. The decrease is more evident in the first ten hours. For the convenience of later discussion we will define the increase of frontal gradient as frontogenesis and the decrease of frontal gradient as frontolysis. The strength of the front is defined as the magnitude of that gradient. In FCL3 and FCL4 the frontal intensity is hold in some extent due to the cold advection behind the front and warm advection before front. Besides there is warm frontogenesis behind the cold front. This mechanism is similar to frontogenesis in two-dimensional baroclinic wave.

4.2 *Topographic effects on fronts*

In order to demonstrate that how a mature front is affected by topography; in this section we compare the results of FCN1, FEX1 and FEX2. Figure 2 shows the potential

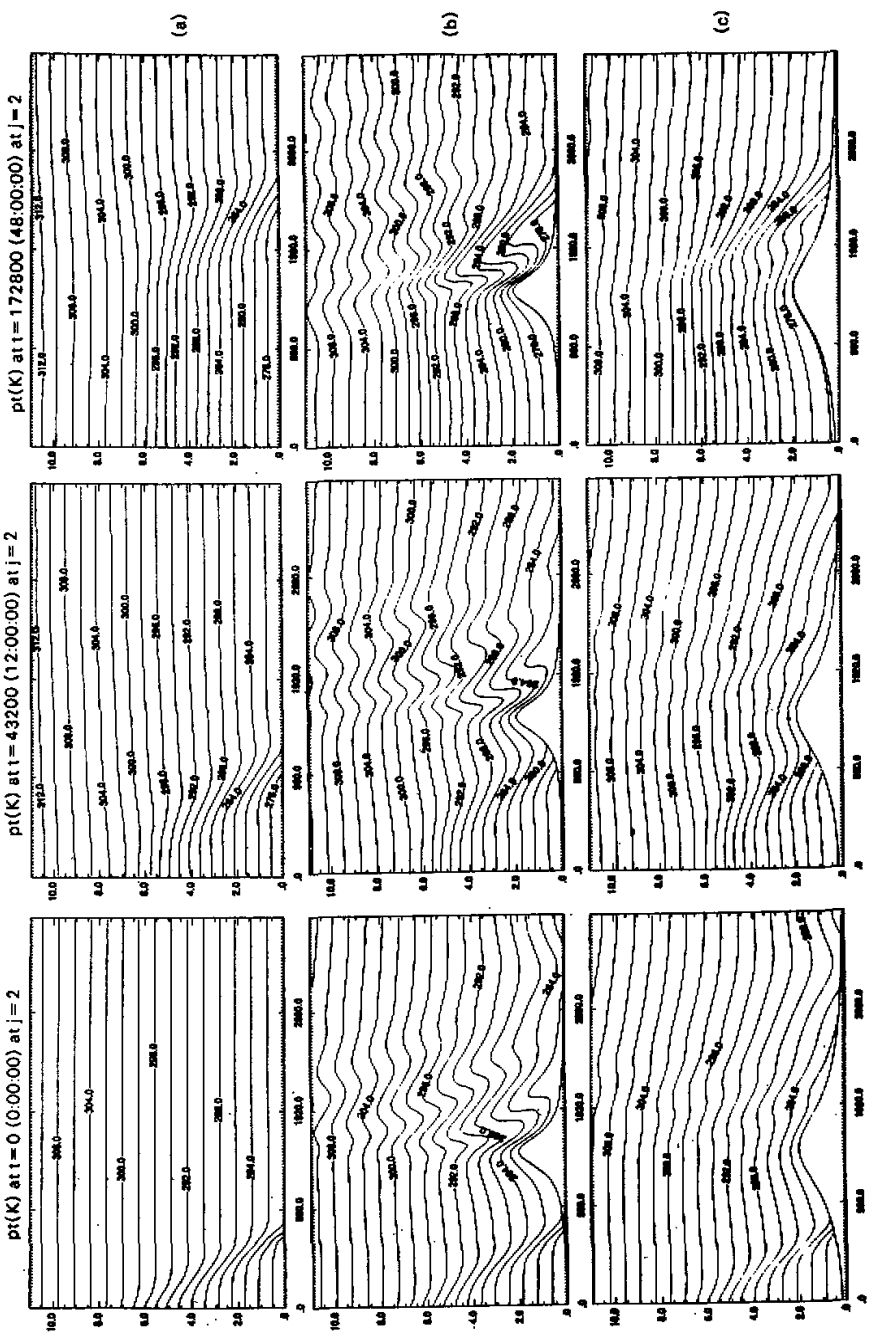

Fig. 2. Isentropes in x–z plane for the cold front and mountain with width 200 km and 500 km. Plots are at $t=0$ h, $t=12$ h, and $t=48$ h for FCL1 (a), FEX1 (b), FEX2 (c) respectively. The mountain ridge is located at $x=1500$ km.

temperature at $t=0$ h, $t=12$ h, and $t=48$ h respectively. The primary modifications of the frontal gradient are through superposition with the orographic gradient. When it is located on the upwind side of the mountain, the superposition weakens the gradient of cold front. There is an increasing of the surface gradient when the front is located downstream of the mountain. Besides the superposition of thermal fields, the dynamic action of orographic disturbance is also evident. Figure 3 shows the horizontal gradient of surface potential temperature variation with time. Although the gradient associated with steady mountain solution is subtracted from it, there is still temporal variation of temperature gradient. This is due to that dynamical action of mountain induced circulation contributes to frontogenesis or frontolysis. The dynamical action of gentle slope mountain ridge (FEX2) weakens cold front on the upwind slope, strengthens cold front slightly on the lee side. And the frontal intensity is strongly increased near the mountain base. While for the steeper slope mountain (FEX1), the dynamical effect weakens the front on the upwind slope, strengthens the front on the mountain top. The frontal intensity is decreased rapidly when the front moves downslope. As the front moves into the convergent zone near the mountain base its intensity is enhanced obviously. When the front has moved away from the mountain area, the final frontal intensity comes back to the value without influence of topography. Compared FEX1 with FEX2, the dynamical action associated with steeper mountain becomes larger. For the topography with the half-width of 200 km the maximum of frontal potential gradient at lee side is 4 K / 100 km, but the maximum of frontal potential gradient is only 2.5 K / 100 km for the mountain with the half-width of 500 km. Besides, as front has passed the narrow mountain ridge, there is an evident oscillation of horizontal gradient of potential temperature at the ridge. It is caused by the interaction of topography with inertia oscillation behind front. This phenomenon will be discussed in detail later.

Some dynamical insights may be obtained from the frontogenetical function. Under the adiabatic assumption, by taking the x-derivative of $\frac{d\theta}{dt}=0$, the individual change of the horizontal potential temperature gradient can be expressed as (Zehnder and Bannon, 1988), i.e.

$$\frac{d}{dt}\left(\frac{\partial\theta}{\partial x}\right)=\underbrace{-\frac{\partial\theta}{\partial x}\frac{\partial u}{\partial x}}_{\mathrm{I}}\underbrace{-\frac{\partial\theta}{\partial y}\frac{\partial v}{\partial x}}_{\mathrm{II}}\underbrace{-\frac{\partial\theta}{\partial z}\frac{\partial w}{\partial x}}_{\mathrm{III}}. \tag{4}$$

The first term (I) on the right-hand side of Eq. (4) is known as the deformation term, it is due to the convergence of the zonal velocity. The second term (II), known as the shear term, is not relevant to FEX1 and FEX1 for barotropic basic flow case, but it is relevant to FEX3 in baroclinic basic flow. The third term (III) is due to differential vertical motion, and known as the tilting term. For the cold front and stable stratification, $\partial\theta/\partial x>0$ and $\partial\theta/\partial z>0$, so there is frontogenesis in the convergent zone and thermal indirect circulation. Changes in the frontal gradient that are not attributed to superposition may be explained in terms of orographic disturbance that is dominated by that component forced by the mountain for the weak front. The mountain forced divergence field given in Fig. 1 shows that there is overall divergence on the upwind slope. On the lee side, there is overall convergence with small divergence area in the valley. The calculation shows that the term I in FEX1 and FEX2 (figure omitted) is frontolysis on the upwind slope. There is frontogenesis on the downwind slope and the lee side convergent zone. The term III indicates that there is frontolysis on the

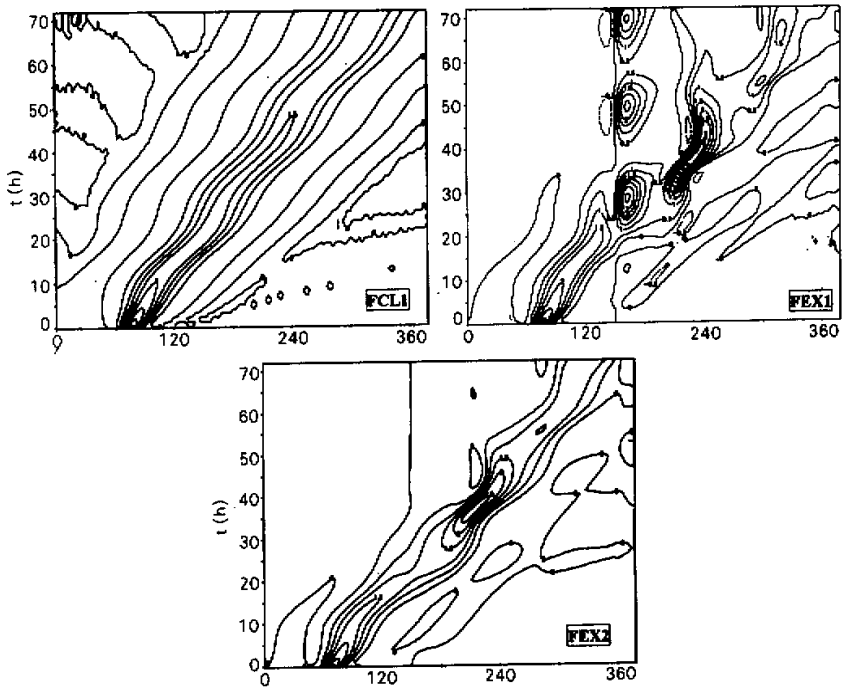

Fig. 3. Isentropes of $\partial\theta / \partial x$ in $x-t$ plane for the cold front (FCL1) and the field for the cold front over mountain subtracted steady mountain solution (FEX1, FEX2). The contour interval is 0.5 K / 100 km.

upwind side where $\partial w / \partial x > 0$. There is frontogenesis on the mountain top where $\partial w / \partial x < 0$ and frontolysis over the downslope where $\partial w / \partial x > 0$. The calculation shows that the term III is predominant over the term I in FEX1. However, in FEX2 the term I is as large as the term III. So for the steep slope mountain the front is frontolysis on the downslope. For the gentle slope mountain the front at the downslope is weak frontogenesis (see Fig. 3). As the front moves to the lee side convergent zone at the mountain foot, the term III near surface ground decreases rapidly, so that the term I is dominant for the frontogenesis. After that the frontal intensity is reduced again by the divergence of mountain wave and the model numerical dissipation.

4.3 *The effects of frontal intensity and baroclinity of airflow on the front over mountain*

Figure 4 shows the horizontal gradient of surface potential temperature varying with time in experiments FEX1, FEX4, FEX3 and FEX5. The gradient associated with steady mountain solution is included in the figure. In FEX1, FEX4 the steady mountain forced solution is just the same as EX1S for barotropic basic flow case. And for baroclinic basic flow case (FEX3, FEX5), the steady mountain forced solution is the same as EX3S. It has shown that there is strong interaction between the orographic disturbance and the front when the front is intensive for both barotropic flow and baroclinic flow. The intensive cold front

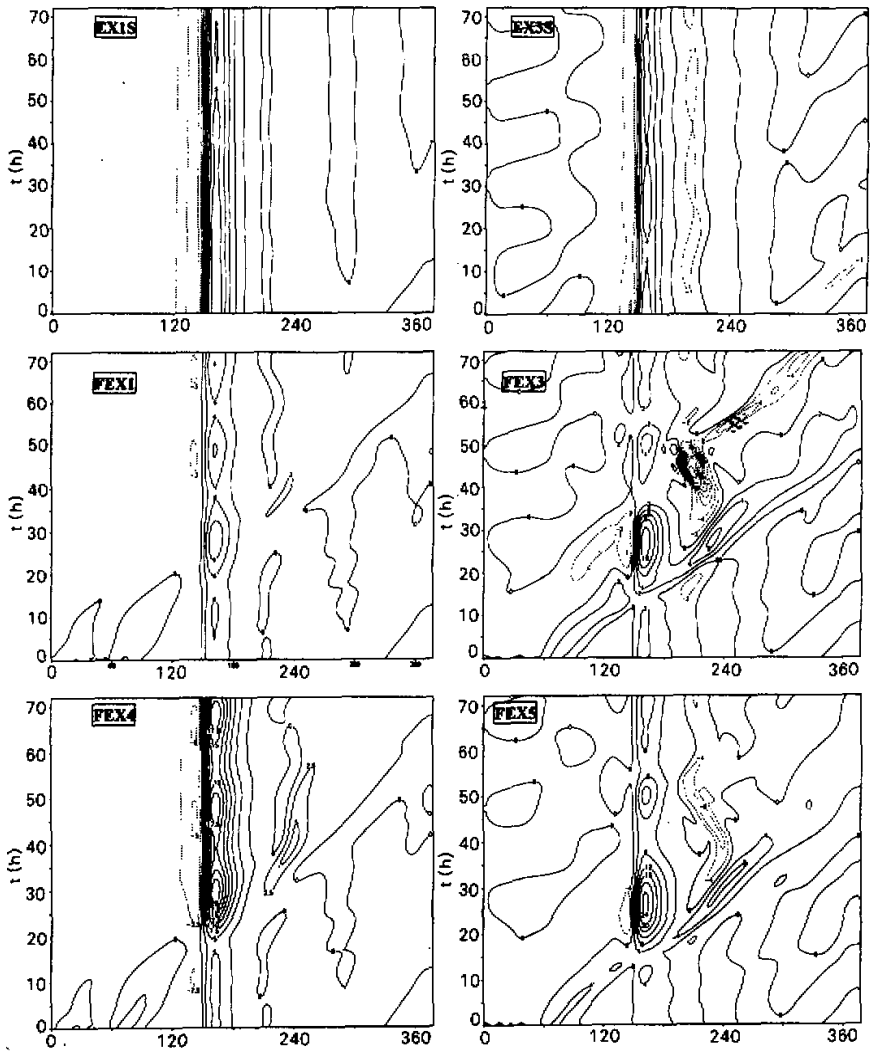

Fig. 4. Isentropes of $\partial\theta / \partial x$ in $x-t$ plane for barotropic and baroclinic flow over mountain (EX1S, EX3S) and different cold fronts over mountain (FEX1, FEX4, FEX3, FEX5).

increases the downslope wind dramatically. The horizontal potential temperature gradient is also changed significantly near the mountain top. When the front is embedded in baroclinic flow ($\partial\theta / \partial y < 0$), the southerly on the upwind side causes the cold front less frontolysis as the cold front approaches the topography. Because on the upwind slope $\partial v / \partial x > 0$, the second term in Eq.(4) is frontogenesis. While the northerly on the lee side causes the clod front severe frontogenesis near the mountain base where $\partial v / \partial x > 0$ is also present.

The magnitude of the maximum wind velocity can indicate the intensity of disturbance in some extent. Figure 5a shows the maximum value of the surface wind as a function of time for

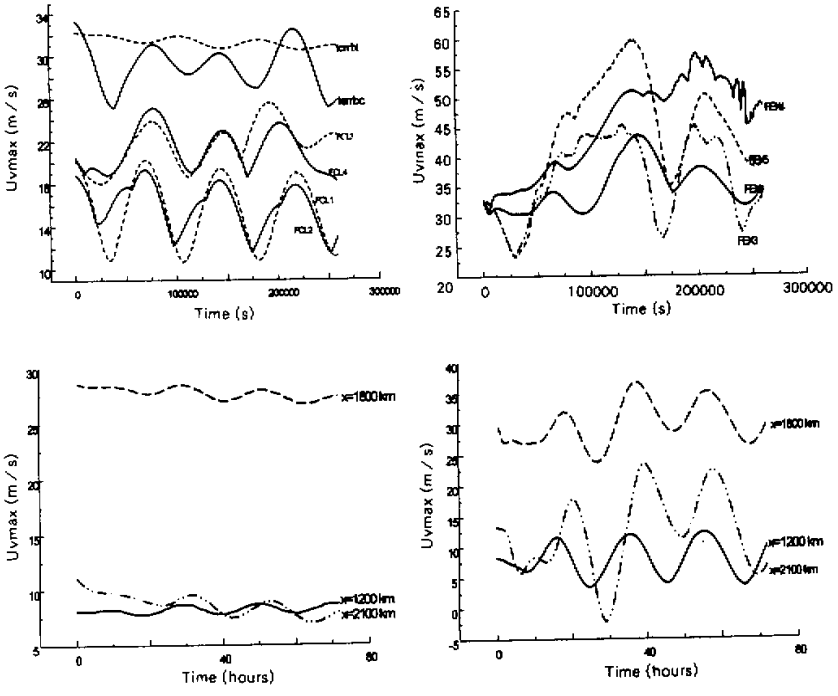

Fig. 5. The maximum surface velocity against time, (a) for the only flow over mountain and only front in the barotropic and baroclinic flow, where the curve symbolized "terrbt" is the barotropic flow over mountain case and curve symbolized "terrbc" is the baroclinic flow over mountain case and the other curves are symbolized with their experiment numbers, (b) for fronts of the different intensities over mountains in the barotropic and baroclinic flow. (c) The inertia oscillation of surface velocity at different positions for only flow over mountain. (d) The inertia oscillation of surface velocity at different positions for front over mountain.

the mountain–only case and front–only case. Figure 5b shows the maximum value of surface wind against time for the frontal interaction with topography. The maximum value usually happens at the downslope flow. The maximum velocities are of few differences for fronts of different intensities in the same basic flow or for mountain–only disturbances. However, if there is interaction of fronts with topography, the amplitude of disturbance increases evidently. For the weak front cases (FEX1 and FEX3) the increase of wind speed is mainly due to superposition effect, but for the strong front cases (FEX4 and FEX5) there are strong interactions between fronts and orographic disturbances. The intensive cold front dramatically increases the downslope wind and lee side gravity wave activity. They will in turn act upon the front and change its intensity, its structure and its propagation speed. Besides, when the intensive front passes down the lee slope, new disturbances are generated and left behind the frontal zone near the base of the mountain. The extreme increase of downslope wind is mostly due to the decrease of Froude number as the intensive front moves over the

mountain.

Comparing FEX1 with FEX4 and FEX3 with FEX5 in Fig. 4, the interaction of front with topography in baroclinic flow is similar to the barotropic case. However, the southerly warm advection on the upwind sides reduces the frontolysis of the cold front, and northerly on the lee side increases frontogenesis at the mountain base. Besides, the warm front caused by cold / warm advection is strengthened on the upwind slope and weakened on the mountain top. The warm front gradient disappears on the downwind slope. As the cold front intensifies on the lee side convergent zone at mountain foot, there is new local warm frontogenesis caused by the strong downslope warming.

4.4 *Effects of topography on the inertia oscillation near the front*

One interesting feature is the inertia oscillation near the front. It can be manifested in the wind speed variation with a period of $2\pi / f \approx 18$ hours. The maximum surface wind in Figs. 5a and 5b has shown this variation. For further analysis, the local wind speed variation with time at three different positions is given in Figs. 5c and 5d. Figure 5c shows the time variation of wind speed at $x=1200$ km, $x=1800$ km and $x=2100$ km for the mountain–only case. The amplitudes are very small in this case. Figure 5d shows the result of FEX1. It is clear that the amplitudes are amplified by the topography. Particularly the amplification is greater at $x=2100$ km than that at other two places. Eliassen and Thorsteinsson (1984) have analyzed the inertia oscillation of airflow over mountain. Blumen et al. (1996) have investigated the inertia oscillation near the front by observational and analytical approaches. In our simulations the inertia oscillation is also evident. Furthermore, it is amplified by the topography on the lee side as the front passes over the mountain. For the narrow mountain the inertia oscillation of surface wind causes the variation of horizontal potential temperature gradient on the top of topography (see Fig. 3 and Fig. 4).

4.5 *Compared with semi–geostrophic results*

The semi–geostrophic results in Zehnder and Bannon (1988) are compared with our results here. They take Gauss type profile of topography of half width 300 km. The deformation field is imposed on their semi–geostrophic model, but the deformation frontogenesis is negligible compared with topographic effects near the topography. Their Fig. 9 shows that the cold front weakens on the upwind slope and the most frontal strengthening area is on the downwind slope near the mountain top when the topographical gradient has been subtracted. Our numerical solutions show that the dynamical action of mesoscale mountain weakens cold front on the upwind slope, strengthens cold front on the mountain ridge. The frontal intensity decreases as the front moves down on the lee side. The maximum intensity of frontal gradient happens in the lee side convergent zone near the mountain base. The maximum frontogenetical region is further downstream than the semigeostrophic result. Another evident difference is that there is strong interaction between the intensive front and the topographic disturbance in the nonhydrostatic model. However, in the semi–geostrophic model, increasing the initial frontal strength does not significantly change the character of the interaction, due to the fact that the value of the ageostrophic stream–function at the surface only depends on the geostrophic zonal wind and the slope of the mountain profile. The frontal strength will make no contribution. For steeper slope mountain, the gravity waves and even a hydraulic jump are observed in the lee side, the vertical structure of the frontal system may be modified by the reversed flow. The semi–geostrophic equations include ageostrophic advections but eliminate the gravity waves, so that the semi–geostrophic equations cannot

describe the effects of lee wave and mountain wave on the front. Even for mountain ridge with half width of 500 km the difference between the semi–geostrophic result and nonhydrostatic model is distinct.

5. Discussion and conclusion

In this paper, a nonhydrostatic fully compressible mesoscale model (ARPS) is used to study the interaction of a mountain ridge with passing mature front. At first, the barotropic and baroclinic flows over mountains with different Froude numbers and Rossby numbers are investigated. The results show that the larger the Rossby number, the larger the departure of the orographic disturbances from the semi–geostrophic mountain steady solution for a given Froude number. For a given Rossby number, the results indicate that the small Froude number is in favor of topographic blocking and strong downslope wind in the lee side. The small Froude number prevents the waves from propagating to higher level, the baroclinic flow is in favor of upward development of disturbances. As the mountain forced flow tends toward to the quasi–steady, the lowest isentrope coincides with the topographic surface and consists of a cold orographic anomaly. The fields are clearly asymmetric with respect to the crest of the ridge with gravity wave activity on the lee side. For the steeper slope mesoscale mountains, the cross–mountain acceleration increases dramatically and the speed maximum is advected down to the lee side slope. When it reaches the base of the topography, a hydraulic jump is generated near the surface.

In the interactive experiments the initial potential temperature perturbation representing the mature front is added to the mountain solution and the model is integrated forward in time. The numerical solutions of frontal interaction with topography show that for the weak front, it is dominated mainly by the orographic disturbance. The thermal superposition reduces frontal intensity as the clod front moves up to the mountain and increases the frontal intensity on the lee side. Conversely, the warm front intensity is increased on the upwind slope and decreased on the downwind slope. The major dynamical mechanism acting on the front is the mountain–forced divergent field and vertical motion. For the mesoscale mountain ridge of gentle slope, the dynamical action weakens cold front on the upwind slope, strengthens cold front on the lee side. This case is consistent with the result of Xiao and Wu et al. (1997). However, for the steeper slope mesoscale mountain, the dynamical effect weakens the front on the upwind slope, strengthens the front on the mountain top, decreases its intensity when front moves downslope rapidly, and increases its intensity as front moves into the convergent zone near the mountain base. This result is evidently different from the semi–geostrophic result in Zehnder and Bannon (1988).

Observations have indicated that the front passing over mountain may cause severe downslope wind and lee cyclogenesis. The numerical results show that there is strong interaction between the orographic disturbance and the intensive front. The intensive cold front dramatically increases the downslope wind and lee side gravity wave activity. The downslope wind and lee side gravity wave activity will in turn act upon the frontal intensity and structure.

Vertical shear of the basic currents should be considered with regard to frontogenetic forcing and mean flow effects. In this study, the baroclinic basic effects have also been investigated. The southerly warm advection on the upwind side weakens the frontolysis, and northerly on the lee side severely intensifies the frontogenesis. Besides, in the baroclinic flow case, there is warm frontogenesis behind the cold front.

In our simulations the inertia oscillation is evident. It is amplified by the topography in the lee side as the front passes over the mountain. For the narrow mountain the inertia oscillation of surface wind causes the horizontal potential temperature gradient variation on the top of topography.

REFERENCES

Bannon, P. R., 1983: Quasi-geostrophic frontogenesis over topography. *J. Atmos. Sci.*, **40**, 2266–2277.

Bannon, P. R., and J. A. Zehnder, 1989: Baroclinic flow over a mountain ridge. *J. Atmos. Sci.*, **46**, 703–714.

Blumen, W., 1992: Propagation of fronts and frontogenesis versus frontolysis over orography. *Meteor. Atmos. Phys.*, **48**, 37–50.

Blumen, W. et al., 1996: The low-level structure and evolution of dry arctic front over the central United States. Part II: comparison with theory. *Mon. Wea. Rev.*, **124**, 1676–1692.

Drazin, P. G., 1961: On the steady flow of a fluid of variable density past an obstacle. *Tellus*, **13**, 239–251.

Eliassen, A., and S. Thorsteinsson, 1984: Numerical studies of stratified airflow over a mountain ridge on the rotating earth. *Tellus*, **36A**, 172–186.

Lu Keli, and Nong Shangyao, 1995: Topography and frontogenesis. *Acta Meteor. Sinica*, **53**, 513–528. (Supplement, in Chinese)

Orlanski, I., and B. B. Ross, 1977: The circulation associated with a cold front. Part I: dry case. *J. Atmos. Sci.*, **34**, 1619–1633.

Queney, P., 1948: The problem of air flow over mountain: A summary of theoretical studies. *Bull. Amer. Meteor. Soc.*, **29**, 16–26.

Smith, R. B., 1986: Mesoscale mountain meteorology in Alps. Scientific Results of the Alpine Experiment, GARP Publications Series, World Meteorological Organization, **3**, 407–423.

Williams, R. T., M. S. Peng, and D. A. Zankofski, 1992: Effects of topography on fronts. *J. Atmos. Sci.*, **49**, 287–305.

Xiao Qingnong, Wu Rongsheng, Zhang Ying, 1997: Dynamic influence of orography on frontogenesis. *Chinese J. Atmos. Sci.*, **21**, 143–150.

Xue Ming, K. K. Droegemeier, V. Wong, A. Shapiro, and K. Brewster, 1995: *ARPS Version 4.0 User's Guide*, Center for Analysis and Prediction of Storm, 380 pp.

Zehnder, J. A., and P. R. Bannon, 1988: Frontogenesis over a mountain ridge. *J. Atmos. Sci.*, **45**, 628–644.

Zhu Qiangen et al., 1992: *Synoptic Meteorology Principle and Method*, China Meteorological Press, 914 pp (in Chinese).